Sinuosity of midlatitude atmospheric flow in a warming world

Julien Cattiaux, Yannick Peings, D Saint-martin, Nadège Trou-Kechout, Stephen Vavrus

AGU PUBLICATIONS

Geophysical Research Letters

RESEARCH LETTER
10.1002/2016GL070309

Key Points:
- The sinuosity is a relevant and intuitive metric to characterize the midlatitude flow waviness in all regions and seasons
- Despite a slight increase observed over recent years, the sinuosity is projected to decrease in CMIP5 climate simulations
- Changes in sinuosity are modulated by the competition between the expansion of tropical Hadley cells and Arctic temperature changes

Supporting Information:
- Supporting Information S1

Correspondence to:
J. Cattiaux,
julien.cattiaux@meteo.fr

Citation:
Cattiaux, J., Y. Peings, D. Saint-Martin, N. Trou-Kechout, and S. J. Vavrus (2016), Sinuosity of midlatitude atmospheric flow in a warming world, *Geophys. Res. Lett.*, *43*, 8259–8268, doi:10.1002/2016GL070309.

Received 14 APR 2016
Accepted 28 JUL 2016
Accepted article online 1 AUG 2016
Published online 15 AUG 2016

Sinuosity of midlatitude atmospheric flow in a warming world

Julien Cattiaux[1], Yannick Peings[2], David Saint-Martin[1], Nadege Trou-Kechout[1], and Stephen J. Vavrus[3]

[1]Centre National de Recherches Meteorologiques, CNRS/Meteo-France, Toulouse, France, [2]Department of Earth System Science, University of California, Irvine, California, USA, [3]Center for Climatic Research, University of Wisconsin-Madison, Madison, Wisconsin, USA

Abstract Global warming is expected to affect midlatitude atmospheric dynamics through changes in the equator-to-pole temperature gradient. While the latitudinal expansion of the tropics would induce both a poleward shift and reinforcement of the westerlies, Arctic changes might counterbalance this effect. Beyond position and speed, potential changes in the flow waviness are crucial for midlatitude weather. Here we investigate such changes through an intuitive metric characterizing the flow sinuosity at 50°N. We find that despite a slight increase in recent reanalyses, the midlatitude sinuosity is projected to decrease in response to climate change according to CMIP5 simulations. Recent trends could therefore result from internal variability or different timings of tropical and polar influences. Future uncertainties are dominated by model discrepancies and partially linked to the dispersion in the equator-to-pole temperature gradient response. Our results support the hypothesis that a faster westerly flow is expected to be less sinuous (and vice-versa).

1. Introduction

Midlatitude synoptic surface climate variability is mostly driven by the atmospheric dynamics [*Lorenz*, 1951]. The unstable nature of the westerly jet stream generates traveling large-scale circulation patterns associated with surface weather anomalies [*Van Loon and Williams*, 1976]. Assessing how climate change may affect inherent fluctuations of the atmospheric dynamics is therefore crucial to understand the response of surface weather, including extreme events.

Both trajectory and speed of the midlatitude flow are related to the strength of the equator-to-pole temperature gradient. Because global warming is latitudinally nonuniform, it can therefore affect the midlatitude flow. But because the meridional temperature gradient is expected to simultaneously increase in the upper troposphere (due to a stronger tropical warming) and decrease near the surface (due to a stronger polar warming), the question of *how* remains wide open [*Held*, 1993]. This particularly holds for the Northern Hemisphere wintertime where the polar warming—i.e., the Arctic Amplification (AA)—is the strongest.

In idealized model experiments, the upper tropospheric tropical warming induces both a poleward shift and a strengthening of the westerly flow—i.e., projects onto the positive phase of the Northern Annular Mode (NAM+)—while the surface polar warming induces the opposite (NAM−) [*Butler et al.*, 2010; *Rivière*, 2011]. In the late 1990s to early 2000s, the former effect was hypothesized to prevail. At that time, this was supported by both a trend in observational data [*Corti et al.*, 1999; *Hsu and Zwiers*, 2001] and a robust signal in climate model projections of the Coupled Model Intercomparison Project (CMIP) [*Gillett et al.*, 2003; *Miller et al.*, 2006]. Since then (i) recent NAM− winters have offset the apparent NAM+ trend [*Cattiaux et al.*, 2010; *L'Heureux et al.*, 2010], and (ii) the latest generation of climate projections (CMIP5) have refuted the systematic NAM+ change found in previous CMIPs [*Cattiaux and Cassou*, 2013; *Barnes and Polvani*, 2015]. In both cases, the AA has been claimed to play a key role [*Overland and Wang*, 2010; *Francis et al.*, 2009; *Cattiaux and Cassou*, 2013]. Particular attention has been drawn to the Arctic sea ice decline, remarkably strong in recent years and faster in CMIP5 than in previous projections [*Stroeve et al.*, 2012]. Some modeling studies have evidenced robust circulation changes when simulating a drastic Arctic sea ice reduction (typically late 21st versus late 20th century conditions) [*Deser et al.*, 2010; *Peings and Magnusdottir*, 2014, among others], but some have failed to find any significant response [*Blackport and Kushner*, 2016; *Semmler et al.*, 2016]. It remains heartily debated whether sea ice trends observed up to now have significantly impacted the midlatitude flow [*Cohen et al.*, 2014; *Screen et al.*, 2013].

Beyond changes in position and speed, a growing interest has been focused on potential changes in the flow waviness, which may directly impact circulation types associated with extreme events (e.g., blockings [*Rex*, 1950]). *Francis and Vavrus* [2012] speculated that a NAM− response to AA should result in a wavier flow favoring the occurrence and/or persistence of blockings, in line with the interannual behavior, and claimed that this was already discernible in recent years [see also, *Francis and Vavrus*, 2015; *Liu et al.*, 2012]. These two points were disputed in *Barnes* [2013] and *Screen and Simmonds* [2013], who highlighted that results on waviness trends were sensitive to the methodology, and *Hassanzadeh et al.* [2014] and *Hassanzadeh and Kuang* [2015], who argued that the NAM− response to AA may rather be associated with a reduced waviness.

Here we revisit these results in the light of a novel metric: the *sinuosity*. This metric is commonly used in geomorphology to quantify river meandering, and we use it here to characterize the sinuosity of the midlatitude flow. Its calculation and validation are presented in section 3. Recent trends and projected changes in sinuosity are assessed in section 4 from the data sets detailed in section 2. Discussion and conclusions are provided in section 5.

2. Data

The sinuosity metric is computed from the 500 mb geopotential height (Z500) which describes the midtropospheric flow. Trends over the recent period are assessed from daily Z500 provided by the ERA-Interim reanalysis data set (hereafter ERAI) over 1979–2014 [*Haylock et al.*, 2008]. We have obtained very similar results with other reanalysis products (not shown). Projected changes are assessed by contrasting periods 1979–2008 and 2070–2099 in historical and future CMIP5 simulations from 24 climate models (Table S1 in the supporting information). In order to maximize the signal, we retain the future scenario with the highest increase in greenhouse gases concentrations, i.e., the 8.5 W m^{-2} Radiative Concentration Pathway (hereafter RCP85). Only one run is used per model (namely the run *r1i1p1*) so that the variance of the CMIP5 ensemble (σ^2_{cmip}) mixes both model uncertainty (σ^2_{mod}) and internal variability (σ^2_{int}). To isolate the internal variability, we also use simulations of the Community Earth System Model-Large Ensemble Project (hereafter CESM-LENS), i.e., 40 historical and RCP85 ensemble members performed with the CESM1 climate model [*Kay et al.*, 2015]. Assuming that $\sigma^2_{cmip} = \sigma^2_{mod} + \sigma^2_{int}$ and that $\sigma_{int} = \sigma_{cesm}$, we compute the ratio

$$\alpha = \frac{\sigma_{mod}}{\sigma_{int}} = \sqrt{\frac{\sigma^2_{cmip}}{\sigma^2_{cesm}} - 1}$$

which indicates whether the CMIP5 dispersion is dominated by model uncertainty ($\alpha > 1$) or internal variability ($\alpha < 1$). Additional monthly variables from both CMIP5 and CESM-LENS experiments are used in section 4.2. All reanalysis and model data sets are first bilinearly interpolated onto a common regular 2.5° × 2.5° longitude-latitude grid in order to allow for a fair comparison.

3. The Sinuosity Metric

3.1. Definition and Example

As done in previous studies [*Barnes*, 2013; *Francis and Vavrus*, 2012, 2015], for each day we characterize the trajectory of the midlatitude flow by isolating a particular 500 mb isohypse (i.e., a line of equal Z500), potentially discontinuous due to cutoff highs and lows (Figure 1a). The value of the selected isohypse is crucial, given that the climatological latitude of a given isohypse (i) fluctuates with the seasonal cycle and (ii) migrates poleward with the Z500 thermal rise induced by global warming. While the former effect can be partially accounted for by using a season-dependent isohypse value (e.g., 5600 m in winter and 5700 m in summer as in *Francis and Vavrus* [2015]), the latter can yield to artificial waviness trends (as demonstrated by *Barnes* [2013]). Here we propose an original technique to account for both effects: for each day, the value of the selected isohypse precisely corresponds to the Z500 average over 30–70°N. By doing so, we insure that we constantly describe the atmospheric flow at the same latitude (approximately 50°N).

Several characteristics of the trajectory can then be computed. Here we primarily focus on the total perimeter of the isohypse to derive the sinuosity but also consider its latitudinal range (maximal and minimal latitudes reached by the isohypse), including potential cutoff highs and lows. We compute these metrics over five domains: the whole Northern Hemisphere and four equally sized subdomains detailed in Figure 1a. To ease

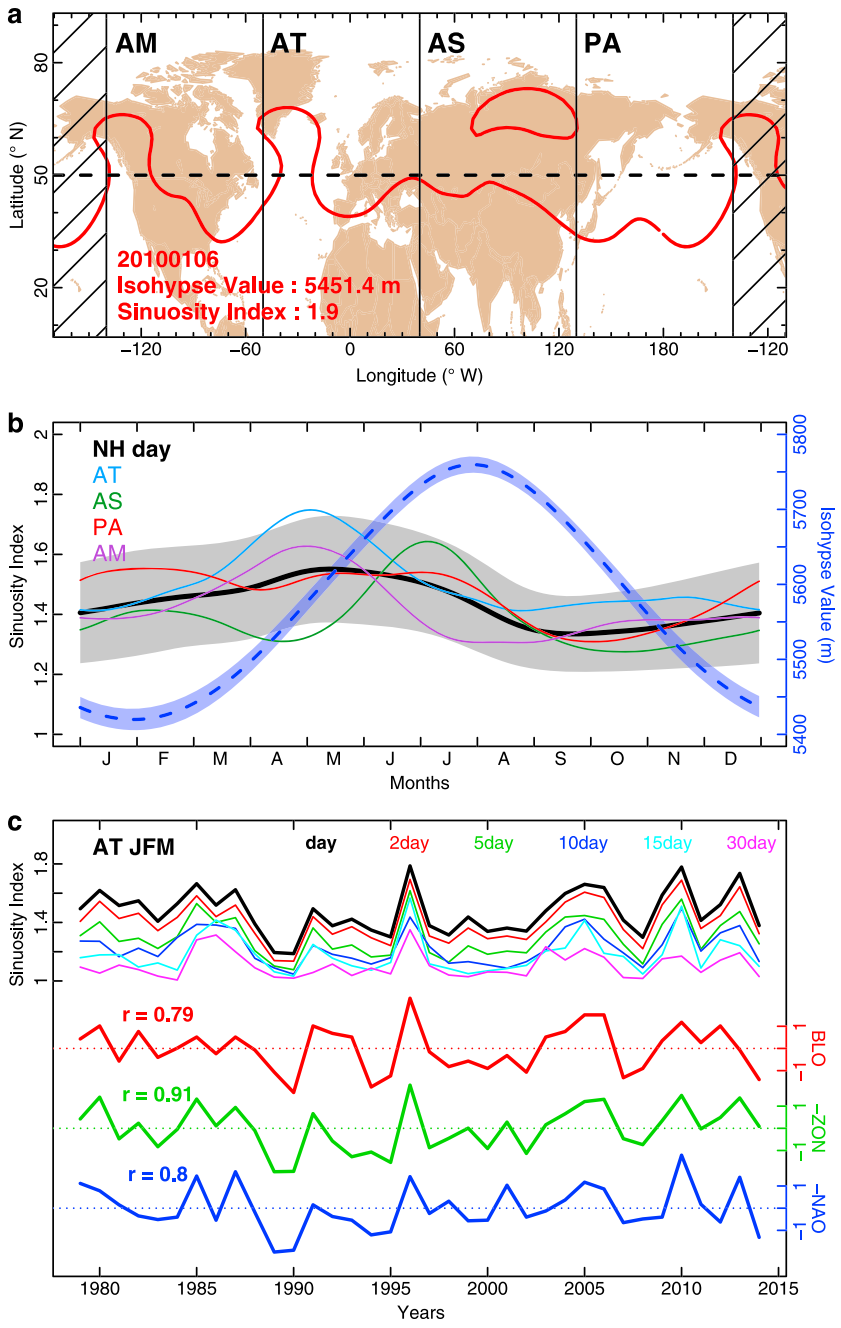

Figure 1. Evaluation of the sinuosity metric in ERAI. (a) Example of the isohypse selected for 6 January 2010 (red line). Isohypse value defined as the Northern Hemisphere (NH) 30–70°N Z500 average. Sinuosity defined as isohypse perimeter divided by the 50°N parallel length. AMerica, ATlantic, ASia, and PAcific subdomains are drawn. (b) Annual cycles of selected isohypse value (dashed blue line), sinuosity for NH (thick black line) and subdomains (colored lines), and respective interannual standard deviations (light blue and gray). (c) Time series of Atlantic winter (January-February-March, JFM) sinuosity for different time scales (see colors) compared to normalized indices of blocking (red), zonal (green), and NAO (blue). Zonal and NAO indices are multiplied by −1 to ease the interpretation. Correlations with daily sinuosity
are indicated.

the interpretation, the perimeter is normalized by the length of the 50°N Earth circle (or quarter circle for subdomains) to derive the sinuosity; a sinuosity equal to 1 thus corresponds to a perfectly zonal isohypse located at 50°N. Finally, the full procedure is repeated on 2 day, 5 day, 10 day, 15 day, and 30 day averages of Z500 to investigate changes in the midlatitude flow at different time scales, from transient small-scale eddies to quasi-stationary large-scale patterns. In practice, we use the functions *contourLines* and *perimeter* of the R package *geosphere*, insuring that the Earth sphericity is accounted for in the perimeter calculation.

Figure 1a provides an illustration of the sinuosity calculation for a given day (6 January 2010). The value of the selected isohypse is 5451.4 m, which corresponds to the 30–70°N Z500 average for this particular day. The sinuosity index is 1.9 for the whole Northern Hemisphere, which is anomalously high (above the 98th percentile of the ERAI January distribution): in addition to a cutoff high in Asia, two strong ridges appear in the American and Atlantic sectors. These conditions were associated with cold spells in Eastern U.S. and Europe [e.g., *Cattiaux et al.*, 2010], illustrating the link between such large-scale circulation meanders and surface weather extremes.

3.2. Evaluation at Seasonal and Interannual Time Scales

Seasonal cycles of both isohypse value and sinuosity indices are shown in Figure 1b. These are derived from ERAI by averaging over all years (1979–2014) for each calendar day and then applying a periodic 30 day spline smoothing. Isohypse values vary from ~5400 m in winter to ~5800 m in summer due to the seasonal migration of the Z500, with only small year-to-year variations. The sinuosity is the highest in spring, mostly due to peaks in the Atlantic and American subdomains, which is consistent with the seasonal cycle of blockings in these sectors (not shown). The sinuosity interannual variability is the largest in winter, when the atmospheric dynamics is the most intense. These seasonal features are not highly sensitive to the latitude used to select the isohypse (here 50°N, see Figures S1e and S1f).

As expected, the sinuosity decreases and gets close to 1 (i.e., zonal flow) when averaging the Z500 field on 2 day, 5 day,…, 30 day blocks prior to compute the index, as illustrated for the Atlantic domain and the winter season in Figure 1c. But year-to-year variations are similar (also true for the full NH domain and, to a lesser extent, for summer, Figures S1c and S1d), suggesting that interannual variability of the daily sinuosity is dominated by large-scale systems rather than small-scale eddies. The sinuosity is also strongly linked to the latitudinal range of the isohypse (Figures S1a and S1b), showing that high sinuosity preferentially results from a few high-amplitude meanders rather than many small-scale oscillations.

Lastly, our sinuosity metric is found to be strongly related to more classical indices used to characterize the wintertime Atlantic dynamics (Figure 1c): we find interannual correlations of (i) −0.8 with the station-based North Atlantic Oscillation (NAO) index provided by the Climate Data Guide (https://climatedataguide.ucar.edu/climate-data/hurrell-north-atlantic-oscillation-nao-index-station-based), (ii) −0.91 with the zonal index defined by *Woollings* [2008] as the Z500 difference between 20–50°N and 60–90°N, and (iii) 0.79 with the Tibaldi-Molteni blocking index (http://www.cpc.ncep.noaa.gov/products/precip/CWlink/blocking/index/index.nh.shtml).

The sinuosity therefore appears as an intuitive metric of the flow waviness, closely related to well-known circulation characteristics in the Atlantic in winter, with the advantage that it can be computed in the exact same way for all seasons and domains (conversely to a NAO index which is specific to the North-Atlantic area and whose definition generally varies from winter to summer).

4. Results

4.1. Recent Trends in ERAI

Here we aim to assess the longest sinuosity trends for all seasons and domains. We therefore search for the oldest year *y* so that the *y*–2014 linear trend is significant at the 90% level. Our null hypothesis is *white noise*, so that our test could be less powerful than a formal detection test accounting for internal variability; however, using the 800 year piControl experiment of the CNRM model (Table S1) to make a proper detection test has given equivalent results (not shown). The statistical procedure is illustrated in Figure 2a for the Atlantic sector in winter: for this particular time series we find that the longest trend is a 29 year increase.

The procedure is then repeated for all seasons and domains (Figure 2b). Only few significant trends arise, and all of them are positive. In particular, we find a significant sinuosity increase at the NH scale in autumn and winter, consistent with *Francis and Vavrus* [2015]. Regionally, there is an increase in the Atlantic during winter

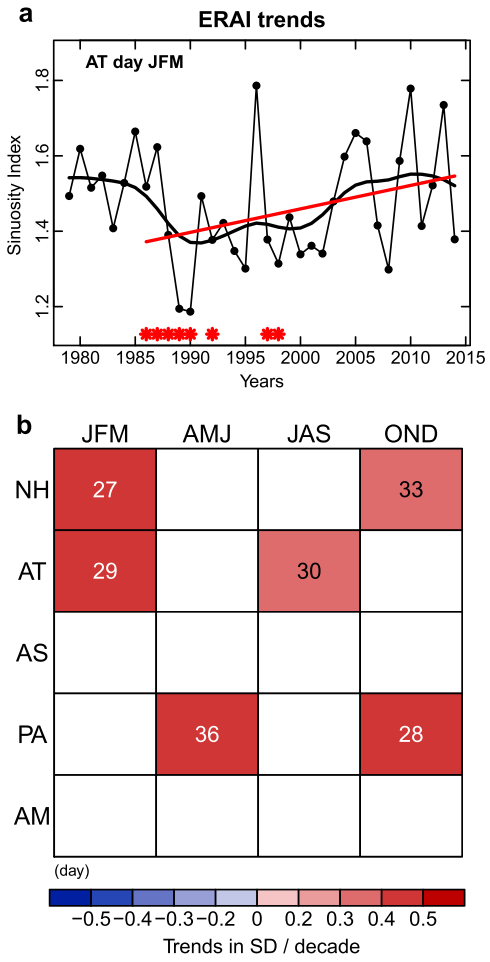

Figure 2. ERAI recent trends in sinuosity. (a) Time series of Atlantic JFM sinuosity, with a 5 year spline smoothing. Red (blue) asterisks are placed at year *y* if a 90%-level significant positive (negative) year is found for period *y*-2014 (here no negative trend is found). The longest significant trend is outlined; trends shorter than 20 years are ignored. (b) Longest significant trends in sinuosity (values in years according to procedure in Figure 2a) for all domains (rows) and seasons (columns). Colors represent trends in standard deviation (SD) per decade.

and summer, and an increase in the Pacific during spring and autumn. These trends are mostly linked to an increase in the maximal latitude reached by the isohypse, rather than to a systematic decrease in minimal latitude (Figure S2). Although not systematic, we generally find similar trends for 5 day or 15 day sinuosity, suggesting a predominant role of large-scale quasi-stationary circulation patterns (Figure S2).

Overall, our analysis highlights the particularly low signal-to-noise ratio for the midlatitude flow, since we only find a few significant trends despite a rather permissive procedure (flexibility for the starting year) and an arbitrarily low confidence level (90%).

4.2. Projected Changes in CMIP5

CMIP5 models simulate the mean sinuosity reasonably well: for all domains and seasons the 24-model HIST ensemble encompasses the 1979–2014 ERAI average and its bootstrapped 95%-level confidence interval, as illustrated for Atlantic and winter in Figure 3a. For raw sinuosity values, the CMIP5 dispersion is largely dominated by model uncertainty (α about 5 to 15 across seasons and domains). To assess projected changes, we ask two distinct questions: (i) do HIST and RCP85 24-model ensemble means significantly differ? and (ii) for each model, do HIST and RCP85 averages of the 30 year time series significantly differ? Both questions are addressed with appropriate *t* tests at 90% level of significance: we compare two samples (HIST versus RCP85) of 24 values for the former (24 models) and 30 values for the latter (30 years per model). In the case of Atlantic during winter, we find that the RCP85 ensemble mean is significantly smaller that HIST, and that this sinuosity decrease is supported by 10 individual models (Figure 3a).

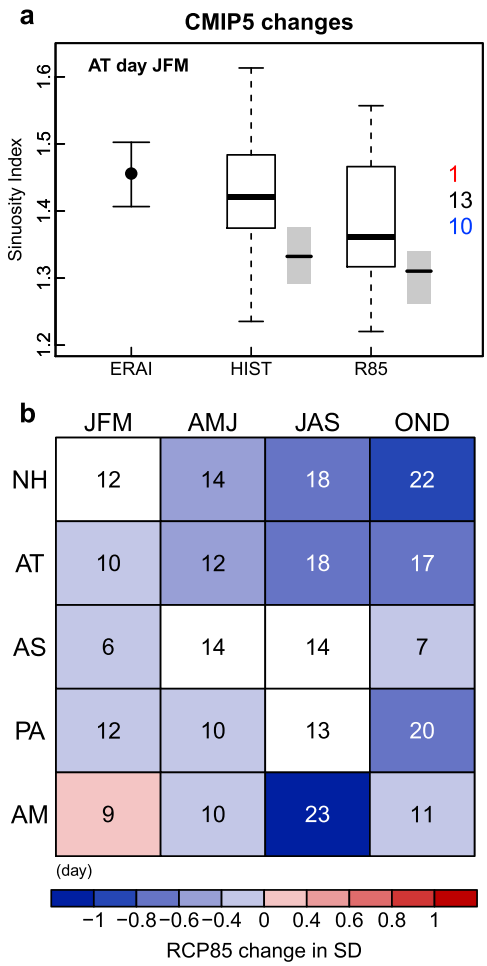

Figure 3. CMIP5 projected changes in sinuosity. (a) Mean of Atlantic JFM daily sinuosity for ERAI, HIST, and RCP85. For ERAI, a 95%-level confidence interval computed by bootstrapping years is added to estimate internal variability. For HIST and RCP85, box plots represent the dispersion of the 24-model ensemble, and numbers of models with a 90%-level significant RCP85-HIST positive (negative) difference are indicated in red (blue). Gray box plots represent the CESM-LENS spread. (b) For all domains (rows) and seasons (columns), red (blue) colors represent 90% level significantly positive (negative) RCP85-HIST ensemble-mean differences in sinuosity. Values represent the number of models individually agreeing with the ensemble-mean difference. The color scale represents the ensemble-mean change in HIST SD units.

The procedure applied to all seasons and domains shows that RCP85 projections suggest a generalized decrease in sinuosity in response to climate change (Figure 3b). The only significant increase is found over America in winter. Over the whole NH, the model agreement on the sign of the change is the largest in summer and autumn and is the poorest in winter, partly due to the competition between the American sector and elsewhere. This is consistent with *Cattiaux et al.* [2013] and *Barnes and Polvani* [2015], who find that the highest uncertainties in the NAM or jet stream response occur in winter. CMIP5 uncertainties in sinuosity changes are overall dominated by model uncertainty, although internal variability can locally have a same order contribution (across seasons, α about 2 to 3 for the whole NH and 1 to 3 for subdomains). The generalized decrease in sinuosity is associated with an increase in the minimum latitude (poleward shift of the southern edge of the isohypse in line with the reported expansion of the tropics), while the decrease in maximum latitude (equatorward shift of the northern edge) is less systematic (Figure S3). These results therefore suggest a meridional narrowing of the midlatitude flow in response to climate change. Similar results are obtained for 5 day or 15 day sinuosity, confirming the predominant role of large-scale quasi-stationary circulation patterns in such long-term changes (Figure S3).

4.3. Link With Changes in the Equator-to-Pole Temperature Gradient

As discussed by *Held* [1993], changes in midlatitude dynamics are expected to result from changes in the vertical profile of the equator-to-pole temperature gradient. CMIP5 simulations project a particularly strong

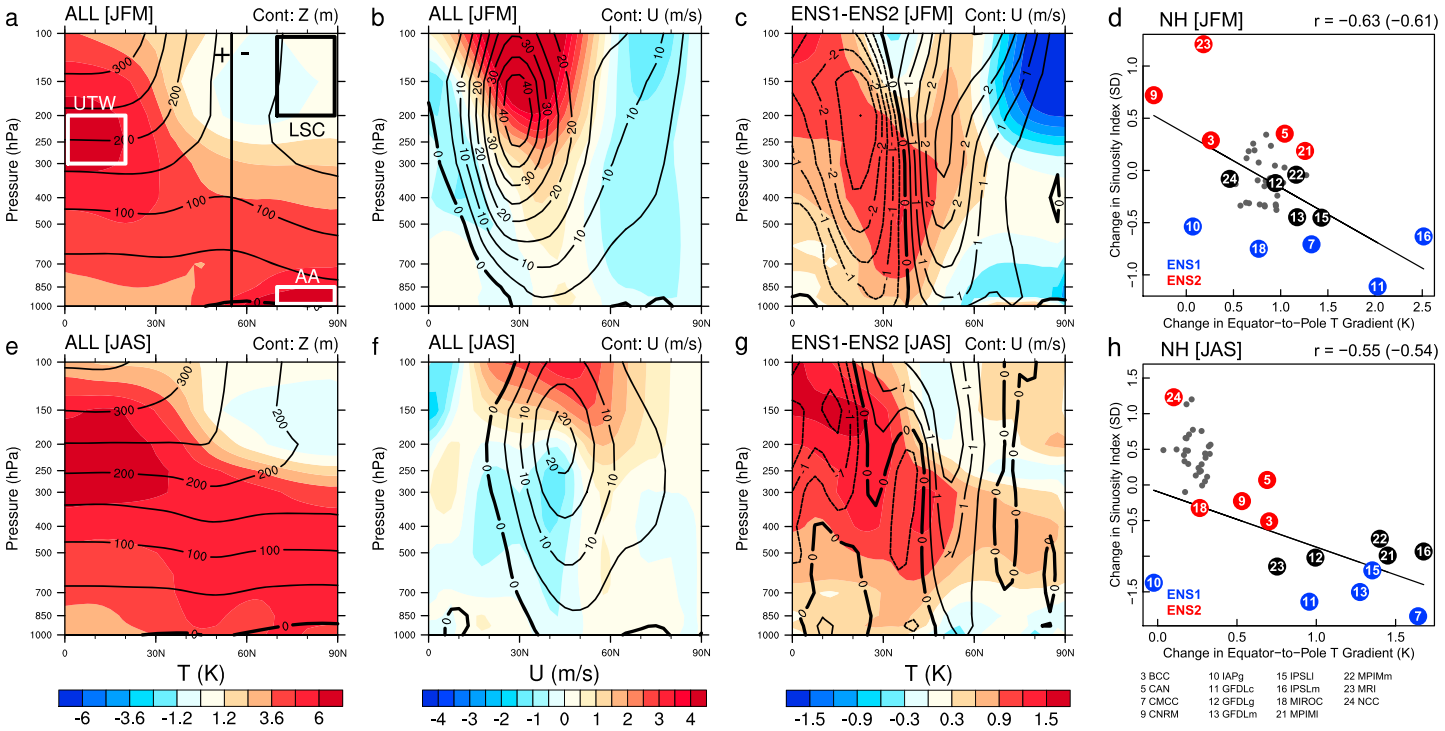

Figure 4. Understanding model dispersion. (a) JFM ensemble-mean RCP85-HIST change in temperature (colors) and geopotential height (contours), zonally averaged over NH. (b) Same for zonal wind (colors) with HIST climatology (contours). (c) Difference in temperature (colors) and zonal wind (contours) changes between two subsets of models: ENS1 (tercile of largest sinuosity decrease) and ENS2 (tercile of weakest sinuosity decrease). (d) Change in NH JFM sinuosity as a function of the change in JFM equator-to-pole temperature gradient. Each numbered circle is a CMIP5 model; ENS1 (ENS2) is indicated in blue (red). Gray dots represent CESM-LENS members. (e–h) Same as Figures 4a–4d for summer (July-August-September, JAS). Only 15 models used due to data availability. UTW, AA, and LSC areas, and the 55°N latitude used for equator-to-pole gradients, are indicated in Figure 4a.

warming in the tropical high troposphere and, especially in winter, in the polar low troposphere (Figures 4a and 4e). Also, a slight cooling spot arises in the polar low-stratospheric area. These temperature changes impact the equator-to-pole temperature gradient and are associated with a poleward shift of both upper jet stream and surface westerlies in summer, while the ensemble-mean zonal wind change rather indicates a narrowing of the westerlies in winter (Figures 4b and 4f).

Simulations with the highest sinuosity decrease also exhibit (i) the strongest tropical upper tropospheric warming (temperature change ΔT in the region defined as 0–20°N/300–200 hPa), (ii) the weakest AA (ΔT in 70–90°N/1000–850 hPa), and, in winter, (iii) the strongest polar low-stratospheric cooling (ΔT in 70–90°N/200–100 hPa, Figures 4c and 4g). Overall, for both seasons the ensemble dispersion in the sinuosity change can be substantially explained by temperature changes: we obtain significant correlations of about −0.6 between the change in sinuosity and a rough index of the change in the equator-to-pole temperature gradient (difference of ΔT between 0–55°N and 55–90°N in the 1000–100 hPa layer), which is strongly model dependent ($\alpha > 5$, Figures 4d and 4h).

In summer, the highest relationship is found with the upper tropospheric warming ($r = 0.3$), whose dispersion almost entirely arises from model uncertainty ($\alpha > 20$). Interestingly, in winter, the highest correlation is found with the polar low-stratospheric cooling ($r = 0.6$). The sign is consistent with traditional intraseasonal stratosphere-troposphere coupling mechanisms, a low-stratospheric cooling being associated with a strengthening of the polar vortex and a more zonal midlatitude flow. The dispersion in winter low-stratospheric temperature response is equally explained by model uncertainty and internal variability ($\alpha \sim 1$).

This suggests that the generalized sinuosity decrease—or narrowing of the midlatitude jet path—mainly results from the latitudinal expansion of the tropics, with a modulation by both AA and polar vortex in winter, the latter being substantially sensitive to internal variability.

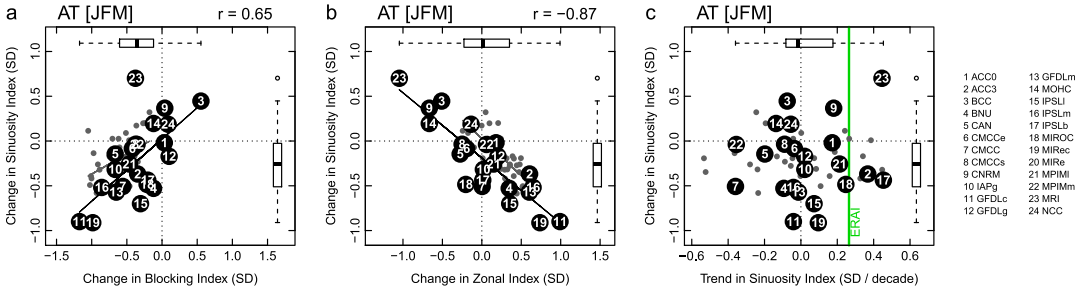

Figure 5. Link with other circulation metrics and recent trends. Change in Atlantic JFM sinuosity as a function of (a) change in blocking index, (b) change in zonal index, and (c) present-day trend in sinuosity. Each numbered circle is a CMIP5 model. Gray dots represent CESM-LENS members. Linear regression is added when significant at the 90% level. Marginal distributions are plotted as box plots. The ERAI trend is added to Figure 5c (green vertical bar).

4.4. Link With Other Circulation Metrics

Beyond the link with temperature changes, Figures 4c and 4g show that simulations with the highest sinuosity decrease also exhibit the strongest poleward shift of both upper level jet stream and surface westerlies. In order to investigate how sinuosity changes relate to responses in other well-known features of large-scale circulation, we calculate zonal and blocking indices used in section 3.2 for HIST and RCP85 simulations. We find that interannual relationships found in Figure 1c in Atlantic in winter also hold for the response to climate change: models with the highest sinuosity decrease also have (i) the highest decrease in blockings and (ii) the highest increase in the zonal index (Figures 5a and 5b). Such intermodel relationships can be generalized to all domains and seasons (Figures S4a and S4b) and support the hypothesis that a less sinuous flow would be stronger (and vice-versa).

The relationship between sinuosity and zonal index (linked to zonal wind) could suggest that changes in sinuosity might be dependent on the latitude chosen for the isohypse selection (here 50°N), since changes in zonal wind depend on latitude (Figures 4b and 4f). We thus verified that the ensemble-mean sinuosity decrease found for all seasons at the NH scale also holds when considering isohypses located at 40, 45, 55, and 60°N (not shown). A more complete analysis of this particular question is left for future studies.

5. Summary and Discussion

This study investigates recent and projected changes in the midlatitude flow waviness in the light of an original and intuitive metric (the sinuosity). Only few significant trends arise across seasons and domains over the period 1979–2014 (strong internal variability), but all of them point toward a wavier flow, consistent with *Francis and Vavrus* [2012, 2015] and *Liu et al.* [2012]. A clearer signal emerges from CMIP5 projections: models project a generalized decrease in midlatitude sinuosity in response to climate change, due to the expansion of the tropics and the meridional narrowing of the flow trajectory. Uncertainties in this response are partially explained by the dispersion in the equator-to-pole temperature gradient response which is highly model dependent. In winter, simulations projecting a larger sinuosity decrease also exhibit a weaker Arctic amplification (AA), a stronger poleward shift of the jet stream, faster westerlies, and a larger decrease in the frequency of blockings. No systematic effect of the horizontal resolution and/or the model lid has been found (not shown). Both recent trends and projected changes in the daily sinuosity are also found for longer time scales (e.g., 5 day and 15 day), suggesting that these signals result from large-scale quasi-stationary circulation patterns rather than from transient synoptic eddies.

Interestingly, sinuosity trends in the CMIP5 ensemble over the HIST period are (i) consistent with the 1979–2014 ERAI value and (ii) not significantly correlated to projected changes (Figures 5c and S4c). This suggests that recently observed trends either result solely from internal variability or are driven by a forcing which is not predominant at the end of the 21st century. For instance, the AA forcing might have dominated the tropical forcing over the recent period, characterized by a fast Arctic sea ice decline, while the tropical forcing might dominate in the late 21st century once the Arctic is nearly ice free and the AA is limited. The competition between effects of greenhouse gases and aerosols might also differ between present-day and future periods; in particular the recent decline in European aerosols might have enhanced the AA [*Navarro et al.*, 2016]. Further research is needed to fully address this issue, including formal detection and attribution

methods applied to recent sinuosity trends, and dedicated model experiments aiming to separate the relative contributions of polar and tropical forcings. Besides, beyond changes in the flow waviness, changes in the persistence of circulation patterns should be further investigated, with potentially greater implications for surface weather extremes.

Acknowledgments
We greatly thank people from CNRM and CERFACS climate groups for useful discussion, particularly F. Chauvin and S. Tyteca for data handling. We acknowledge the World Climate Research Programme's Working Group on Coupled Modelling, which is responsible for CMIP, and we thank the climate modeling groups involved for producing and making available their model output (http://pcmdi9.llnl.gov/esgf-web-fe/). This work was supported by the French ANR MORDICUS project.

References

Barnes, E. (2013), Revisiting the evidence linking Arctic amplification to extreme weather in midlatitudes, *Geophys. Res. Lett.*, *40*(17), 4734–4739, doi:10.1002/grl.50880.

Barnes, E., and L. Polvani (2015), CMIP5 projections of Arctic amplification, of the North American/North Atlantic circulation, and of their relationship, *J. Clim.*, *28*(13), 5254–5271, doi:10.1175/JCLI-D-14-00589.1.

Blackport, R., and P. Kushner (2016), The transient and equilibrium climate response to rapid summertime sea ice loss in CCSM4, *J. Clim.*, *29*(2), 401–417, doi:10.1175/JCLI-D-15-0284.1.

Butler, A., D. Thompson, and R. Heikes (2010), The steady-state atmospheric circulation response to climate change-like thermal forcings in a simple general circulation model, *J. Clim.*, *23*(13), 3474–3496, doi:10.1175/2010JCLI3228.1.

Cattiaux, J., and C. Cassou (2013), Opposite CMIP3/CMIP5 trends in the wintertime Northern Annular Mode explained by combined local sea ice and remote tropical influences, *Geophys. Res. Lett.*, *40*(14), 3682–3687, doi:10.1002/grl.50643.

Cattiaux, J., R. Vautard, C. Cassou, P. Yiou, V. Masson-Delmotte, and F. Codron (2010), Winter 2010 in Europe: A cold extreme in a warming climate, *Geophys. Res. Lett.*, *37*, L20704, doi:10.1029/2010GL044613.

Cattiaux, J., H. Douville, and Y. Peings (2013), European temperatures in CMIP5: Origins of present-day biases and future uncertainties, *Clim. Dyn.*, *41*(11–12), 2889–2907, doi:10.1007/s00382-013-1731-y.

Cohen, J., et al. (2014), Recent Arctic amplification and extreme mid-latitude weather, *Nat. Geosci.*, *7*(9), 627–637, doi:10.1038/ngeo2234.

Corti, S., F. Molteni, and T. Palmer (1999), Signature of recent climate change in frequencies of natural atmospheric circulation regimes, *Nature*, *398*(6730), 799–802, doi:10.1038/19745.

Deser, C., R. Tomas, M. Alexander, and D. Lawrence (2010), The seasonal atmospheric response to projected arctic sea ice loss in the late twenty-first century, *J. Clim.*, *23*, 333–351, doi:10.1175/2009JCLI3053.1.

Francis, J., and S. Vavrus (2012), Evidence linking Arctic amplification to extreme weather in mid-latitudes, *Geophys. Res. Lett.*, *39*(6), L06801, doi:10.1029/2012GL051000.

Francis, J., and S. Vavrus (2015), Evidence for a wavier jet stream in response to rapid Arctic warming, *Environ. Res. Lett.*, *10*(1), 014005, doi:10.1088/1748-9326/10/1/014005.

Francis, J., W. Chan, D. Leathers, J. Miller, and D. Veron (2009), Winter Northern Hemisphere weather patterns remember summer Arctic sea-ice extent, *Geophys. Res. Lett.*, *36*(7), L07503, doi:10.1029/2009GL037274.

Gillett, N., F. Zwiers, A. Weaver, and P. Stott (2003), Detection of human influence on sea-level pressure, *Nature*, *422*(6929), 292–294, doi:10.1038/nature01487.

Hassanzadeh, P., and Z. Kuang (2015), Blocking variability: Arctic amplification versus Arctic oscillation, *Geophys. Res. Lett.*, *42*(20), 8586–8595, doi:10.1002/2015GL065923.

Hassanzadeh, P., Z. Kuang, and B. Farrell (2014), Responses of midlatitude blocks and wave amplitude to changes in the meridional temperature gradient in an idealized dry GCM, *Geophys. Res. Lett.*, *41*(14), 5223–5232, doi:10.1002/2014GL060764.

Haylock, M., N. Hofstra, A. Klein Tank, E. Klok, P. Jones, and M. New (2008), A European daily high-resolution gridded data set of surface temperature and precipitation for 1950–2006, *J. Geophys. Res.*, *113*(20), 119, doi:10.1029/2008JD10201.

Held, I. (1993), Large-scale dynamics and global warming, *Bull. Am. Meteorol. Soc.*, *74*(2), 228–241.

Hsu, C., and F. Zwiers (2001), Climate change in recurrent regimes and modes of Northern Hemisphere atmospheric variability, *J. Geophys. Res.*, *106*(D17), 20,145–20,159, doi:10.1029/2001JD900229.

Kay, J., et al. (2015), The Community Earth System Model (CESM) large ensemble project: A community resource for studying climate change in the presence of internal climate variability, *Bull. Am. Meteorol. Soc.*, *96*(8), 1333–1349, doi:10.1175/BAMS-D-13-00255.1.

L'Heureux, M., A. Butler, B. Jha, A. Kumar, and W. Wang (2010), Unusual extremes in the negative phase of the Arctic oscillation during 2009, *Geophys. Res. Lett.*, *37*(10), L10704, doi:10.1029/2010GL043338.

Liu, J., J. Curry, H. Wang, M. Song, and R. Horton (2012), Impact of declining Arctic sea ice on winter snowfall, *Proc. Natl. Acad. Sci.*, *109*(11), 4074–4079, doi:10.1073/pnas.1114910109.

Lorenz, E. (1951), Seasonal and irregular variations of the Northern Hemisphere sea-level pressure profile, *J. Meteorol.*, *8*(1), 52–59.

Miller, R., G. Schmidt, and D. Shindell (2006), Forced annular variations in the 20th century Intergovernmental Panel on Climate Change fourth assessment report models, *J. Geophys. Res.*, *111*, D18101, doi:10.1029/2005JD006323.

Navarro, J., V. Varma, I. Riipinen, Ø. Seland, A. Kirkevåg, H. Struthers, T. Iversen, H. Hansson, and A. Ekman (2016), Amplification of Arctic warming by past air pollution reductions in Europe, *Nat. Geosci.*, *9*, 277–281, doi:10.1038/ngeo2673.

Overland, J., and M. Wang (2010), Large-scale atmospheric circulation changes are associated with the recent loss of Arctic sea ice, *Tellus, Ser. A*, *62*(1), 1–9, doi:10.1111/j.1600-0870.2009.00421.x.

Peings, Y., and G. Magnusdottir (2014), Response of the wintertime Northern Hemisphere atmospheric circulation to current and projected Arctic sea ice decline: A numerical study with CAM5, *J. Clim.*, *27*(1), 244–264, doi:10.1175/JCLI-D-13-00272.1.

Rex, D. (1950), Blocking action in the middle troposphere and its effect upon regional climate, *Tellus*, *2*(3), 196–211.

Rivière, G. (2011), A dynamical interpretation of the poleward shift of the jet streams in global warming scenarios, *J. Atmos. Sci.*, *68*(6), 1253–1272, doi:10.1175/2011JAS3641.1.

Screen, J., and I. Simmonds (2013), Exploring links between Arctic amplification and mid-latitude weather, *Geophys. Res. Lett.*, *40*(5), 959–964, doi:10.1002/grl.50174.

Screen, J., I. Simmonds, C. Deser, and R. Tomas (2013), The atmospheric response to three decades of observed Arctic sea ice loss, *J. Clim.*, *26*(4), 1230–1248, doi:10.1175/JCLI-D-12-00063.1.

Semmler, T., L. Stulic, T. Jung, N. Tilinina, C. Campos, S. Gulev, and D. Koracin (2016), Seasonal atmospheric responses to reduced Arctic sea ice in an ensemble of coupled model simulations, *J. Clim.*, doi:10.1175/JCLI-D-15-0586.1, in press.

Stroeve, J., V. Kattsov, A. Barrett, M. Serreze, M. Pavlova, and W. Meier (2012), Trends in Arctic sea ice extent from CMIP5, CMIP3 and observations, *Geophys. Res. Lett.*, *39*(16), L16502, doi:10.1029/2012GL052676.

Van Loon, H., and J. Williams (1976), The connection between trends of mean temperature and circulation at the surface: Part I. winter, *Mon. Weather Rev.*, *104*(4), 365–380.

Woollings, T. (2008), Geophys. Res. Lett., *Vertical structure of anthropogenic zonal-mean atmospheric circulation change*, *35*(19), L19702, doi:10.1029/2008GL034883.